Active and Intelligent Control onto Thermal Behaviors of Motorized Spindle Unit

Yifan Zhang[1, 3], Ping Wang[3], Teng Liu[1, 2*], Weiguo Gao[2], Wenfen Chang[2, 4], Yanling Tian[2, 5], and Dawei Zhang[2]

[1] *School of Mechanical Engineering, Hebei University of Technology, Tianjin 300130, China*

[2] *Key Laboratory of Mechanism Theory and Equipment Design of Ministry of Education, Tianjin University, Tianjin 300355, China*

[3] *School of Electrical and Information Engineering, Tianjin University, Tianjin 300072, China*

[4] *Beijing Precision Machinery & Engineering Research Co., Ltd., Beijing 101312, China*

[5] *School of Engineering, University of Warwick, Coventry, CV4 7AL, UK*

Abstract: Motorized spindle unit is the core component of precision CNC machine tool. Its thermal errors perform generally serious disturbance onto the accuracy and accuracy stability of precision machining. Traditionally, the effectiveness of the compensation method for spindle thermal errors is restricted by machine freedom degrees. For this problem, this paper presents an active, differentiated and intelligent control method onto spindle thermal behaviors, to realize comprehensive and accurate suppressions onto spindle thermal errors. Firstly, the mechanism of spindle heat generation / dissipation - structural temperature - thermal deformation error is analyzed. This modeling conveys that the constantly least spindle thermal errors can be realized by differentiated and active controls onto its structural thermal behaviors. Based on this principle, besides, the active control method is developed by a combination of extreme learning machine (ELM) and genetic algorithm (GA). The aim is to realize the general applicability of this active and intelligent control algorithm, for the spindle time-varying thermal behaviors. Consequently, the contrasting experiments clarify that the proposed active and intelligent control method can suppress accurately and synchronously all kinds of spindle thermal errors. It is significantly beneficial for the improvements of the accuracy and accuracy stability of motorized spindle units.

Keywords: Active and intelligent control, Motorized spindle unit, Thermal errors, ELM (Extreme learning machine), GA (Genetic algorithm)

∗E-mail address of the corresponding author: wuqiu-liu@163.com

1 Introduction

In recent years, the application of the motorized spindle unit has significantly increased machining productivity and reduced manufacturing cost. Unfortunately, its high rotation speed and compact structure lead to some negative effects onto spindle thermal behaviors, which have time-varying disturbances onto machine accuracy and accuracy stability. As described in Fig. 1, heat generations with uncertainties from spindle motor and bearings can generally impact temperature behaviors of a motorized spindle unit in its operation, and result in spindle thermal errors. That is the critical reason for the degradation of precision machining accuracy and accuracy stability [1]. Based on this background, the application of intelligent methods onto the regulations for spindle thermal behaviors is necessary for improving accuracy and accuracy stability of precision machining activities. As revealed from the related published contributions, the intelligent control studies onto spindle thermal behaviors mainly include 2 aspects: the construction of intelligent control strategy and the realization of intelligent control method.

In order to construct effectively the intelligent control strategy for spindle thermal behaviors, either physically-based or data-driven models were employed by scholars. On one hand, the physically-based models can be generally represented with computational models, which have been widely established by finite element method (FEM), finite difference method (FDM) and so on. Holkup et al. [2] considered the spindle circulating coolant heat transfer as the forced heat convection, and established the thermal-structure coupling simulation model of the high-speed precision spindle to predict and analyze the spindle transient thermal errors. Jiang et al. [3] used FEM to analyze spindle structural temperature distribution, and the variable spindle preload was determined based on bearing temperature rise constraint at high speed range. At low speed range, the spindle preload was resolved by bearing fatigue life. Then the dynamic stiffness of the variable preload spindle was analyzed for spindle thermal error modeling. Creighton et al. [4] conducted the numerical simulations to get the temperature distribution and thermal growth of a high speed micro milling spindle, with its bearings supporting and motor being considered approximately as main heat sources. Zheng et al. [5] developed a thermal model for high speed press system based on the fractal model and variable heat generation power by FEM, to explore its temperature histories and the time for thermal errors of spindle equilibrium condition. Ma et al. [6] established the theoretical and simulation model of spindle thermal resistance - bearing stiffness to improve the model accuracy of spindle structural temperature and thermal error predictions. Liu et al [7] presented a thermal resistance network model of spindle-bearing conjunction in spindle thermal FE modeling, in order to analyze accurately spindle temperature and thermal errors. These studies tried to establish physical models of spindle thermal behaviors. However, for their low efficiency and accuracy, they were widely used as prior knowledge, rather than the constructed strategy, for the intelligent control realization onto spindle thermal behaviors.

On the other hand, data-driven models for spindle thermal behaviors were widely studied by experiments, to construct intelligent control strategy for spindle thermal behaviors. Recently, some studies improved traditional experimental methods to establish relationships between spindle structural temperatures and thermal errors. Denis Ashok et al. [8] employed the curve fitting theory to establish the spindle temperature - radial thermal error model based on the electric spindle test platform, having reduced the experimental deviation of spindle error prediction caused by its thermal drift. Prashanth Anandan et al. [9] adopted the Laser Doppler Vibrometer technique to measure the radial and axial motions of the miniature ultra-high-speed spindle, from a sphere-on-stem precision artifact. The aim was to experimentally analyze temperature fluctuation influences onto spindle thermal errors, dynamically-induced effects, contact-bearing defects, and tool-attachment errors. Ibaraki et al. [10] proposed an experimental method to observe spindle thermal errors, and analyzed the thermal deformation influence onto error motions of rotary axes change, mainly based on machining test method. Huang et al. [11] applied neural network - genetic algorithm methods to effectively get the accurate compensation model of spindle thermal error. Wang et al. [12] built up an experimental spindle structural temperature - thermal error model, with a sufficient hysteresis and dynamic consideration of solid thermal deformation. Li et al. [13] adopted multiple regression and back propagation network methods to associate spindle thermal errors with its temperature, rotation speed, historical temperature, historical thermal error, and time lag between the present and previous times. Although models established experimentally have widespread applications for intelligent control realizations onto spindle thermal behaviors, unsatisfactory accuracies and universalities of the constructed control strategy influence negatively the suppression effectiveness of spindle thermal errors.

Based on the constructions of intelligent control strategy for spindle thermal behaviors above, some other studies placed emphasis on its realization method based on various sorts of spindle units. Traditionally, spindle thermal errors were mainly minimized by the compensation method, whose main idea was to create an opposite error to eliminate the original spindle thermal error [14-16]. Chang et al. [17] proposed a direct displacement measuring system to accurately monitor and compensate thermal growth associated with the motorized high speed spindles. This system optimizing a high speed synchronous feedback system can meet the tolerance and performance of the spindle high speed machining. Shen et al. [18] developed the on-line asynchronous compensation method for static/quasi-static error caused by thermal deformation and machine geometry, to reduce the complexity and improve the effectiveness of thermal error compensation for motorized spindle unit. Gomez-Acedo et al. [19] presented an experimentally identified model based on a large gantry-type milling machine for compensating spindle thermal errors. The model inputs are spindle speed, temperatures of main motor gearbox and room air, and outputs are estimations of the thermal drift of the machine tool center point along the 3 axes in different positions within the working volume. Yang et al. [20] implemented a thermal error compensation method for a high-speed motorized spindle. His method took the length of cutting tools and thermal angular angles into account in some degrees. Mayr et al. [21] presented a dynamic gray box model based compensation approach for thermal errors induced by the machine rotary and swiveling axis unit as well as the motorized spindle unit. For this compensation model, input parameters are designed to be related to machine heat generation and cooling power, for the compensation improvement of machine dominant thermal errors. Liu et al. [22] tested the radial thermal drift error in Y-direction and temperatures in spindle structural key points of a vertical machining center using its different rotating speeds, for the establishment of radial thermal drift error models under different postures. Although these compensation studies have advantages in the reduction of spindle thermal errors, their effectiveness can generally be influenced by the inaccuracies of the constructed control strategies above. Besides, being the inherent shortage of compensation method, its inability to compensate for spindle thermal errors in the freedom degrees excluded by machine drive system is disadvantageous to the improvements of machine accuracy and accuracy stability as well.

In order to realize the accurate reductions for all kinds of spindle thermal errors, this paper proposes an active, differentiated and intelligent control method onto thermal behaviors of motorized spindle unit. By this method, spindle thermal errors can be comprehensively and consistently suppressed based on the stabilizing regulation onto spindle structural temperature.

The remainder of the paper is organized as follows: Section 2 gives the analytical descriptions about behaviors of spindle structural temperature and thermal deformation errors. Based on their theoretical associations, Section 3 constructs the active and intelligent control strategy algorithm onto spindle thermal behaviors based on ELM-GA method, to realize comprehensive suppressions onto spindle thermal errors. Section 4 reports the experimental methods and results for advantageous verifications of this active and intelligent control method onto spindle thermal behaviors. Section 5 concludes this study as a whole.

2 Analytical bases for active and intelligent control method onto spindle thermal behaviors

This section theoretically analyzes the temperature and thermal error mechanisms based on a simplified spindle structure. These are necessary preparations for the presentation of the active and intelligent control method onto thermal behaviors of motorized spindle unit.

This paper presents a typical physical structure of motorized spindle unit, which is illustrated in Fig. 2: Main heat generating parts of an operating spindle unit are its front bearings (angular contact ball bearings), back bearing (short cylindrical roller bearing) and built-in motor (including stator and rotator). Generally, their heat generations are root reasons for the occurrence of spindle thermal deformation errors. Thus for dissipations of these internal heat generations, helical channels are designed nearby these spindle heat generating parts respectively to realize coolant forced convections. In this section, this spindle structure is simplified to be the assembly of front bearings, motor, back bearing and shaft. The aim is to analyze the interaction relationship of the spindle heat generations, dissipations and conductions, and then to investigate their theoretical association with spindle thermal deformation behaviors.

2.1 Analytical modeling for spindle thermal behaviors

2.1.1 Analytical modeling for spindle heat generation/ dissipation - structural temperature

The spindle structure is simplified to analyze its structural heat exchange, which is revealed in Fig. 3: During a spindle operation in the precision machining environment, heat conductions from spindle front bearings, motor and back bearing $\Phi_{\text{con\_Fr/Mo/Ba}}$ (W) are closely associated with their heat generations $\Phi_{\text{gen\_Fr/Mo/Ba}}$ (W) and heat dissipations $\Phi_{\text{coo\_Fr/Mo/Ba}}$ (W) caused by coolants. These 3 factors mainly impact the temperature behaviors of spindle front bearings, motor and back bearing $T_{\mathrm{Fr/Mo/Ba}}$ (℃), and then determine the spindle structural temperature behaviors. It is assumed that the initial spindle structural temperature is equal to the ambient temperature of precision machining workshop T_{am} (=20℃). Then according to the energy conservation law, relative temperatures $\Delta T_{\mathrm{Fr/Mo/Ba}}\left(=T_{\mathrm{Fr/Mo/Ba}}-T_{\mathrm{am}}\right)$ of spindle heat generating parts are analyzed to be:

$$\Phi_{\mathrm{gen}\_i}-\Phi_{\mathrm{coo}\_i}+\Phi_{\mathrm{con}\_i}=c_{\mathrm{T}\_i}\frac{\mathrm{d}\Delta T_i}{\mathrm{d}\tau}, i=\mathrm{Fr},\mathrm{Mo},\mathrm{Ba} \tag{1}$$

In equation (1), $c_{\mathrm{T\_Fr/Mo/Ba}}$ are heat capacitance values of spindle heat generating parts (J/℃), and their heat conductions ($\Phi_{\mathrm{con\_Fr/Mo/Ba}}$) through the cross sections of the spindle continuous material can be expressed as:

$$\Phi_{\mathrm{con}\_i}=\lambda_i S_i\frac{\mathrm{d}\Delta T_i}{\mathrm{d}x}, i=\mathrm{Fr},\mathrm{Mo},\mathrm{Ba} \tag{2}$$

In equation (2), $S_{\mathrm{Fr/Mo/Ba}}$ are the areas perpendicular to heat flux directions (m^2); $\lambda_{\mathrm{Fr/Mo/Ba}}$ are thermal conductivities of spindle heat generating parts (W/(m•℃)). Meanwhile, the heat dissipations ($\Phi_{\mathrm{coo\_Fr/Mo/Ba}}$) in equation (1) can be approximately seen as applied coolant forced convection effects onto spindle heat generating parts. According to the Newton cooling law, $\Phi_{\mathrm{coo\_Fr/Mo/Ba}}$ can be:

$$\Phi_{\mathrm{coo}\_i}=h_{\mathrm{coo}\_i}\Omega_i(\Delta T_i-\Delta T_{\mathrm{coo}\_i}), i=\mathrm{Fr},\mathrm{Mo},\mathrm{Ba} \tag{3}$$

In equation (3), $\Delta T_{\mathrm{coo\_Fr/Mo/Ba}}\left(=T_{\mathrm{coo\_Fr/Mo/Ba}}-T_{\mathrm{am}}\right)$ are the relative coolant supply temperatures onto spindle heat generating parts, and $h_{\mathrm{coo\_Fr/Mo/Ba}}(\mathrm{w/(m^2\cdot K)})$ are heat transfer coefficients of coolant forced convections, $\Omega_{\mathrm{Fr/Mo/Ba}}$ are areas being perpendicular to heat flux directions (m^2).

Equations (2) and (3) can be substituted into equation (1) to establish the relationship:

$$\frac{\Phi_{\mathrm{gen}\_i}}{h_{\mathrm{coo}\_i}\Omega_i}+\Delta T_{\mathrm{coo}\_i}=\frac{c_{\mathrm{T}\_i}}{h_{\mathrm{coo}\_i}\Omega_i}\bullet\frac{\mathrm{d}\Delta T_i}{\mathrm{d}\tau}+\Delta T_i-\frac{\lambda_i S_i}{h_{\mathrm{coo}\_i}\Omega_i}\bullet\frac{\mathrm{d}\Delta T_i}{\mathrm{d}x}, i=\mathrm{Fr},\mathrm{Mo},\mathrm{Ba} \tag{4}$$

On one hand, $\frac{\mathrm{d}\Delta T_i}{\mathrm{d}x}=0\left(i=\mathrm{Fr},\mathrm{Mo},\mathrm{Ba}\right)$ can be considered in equation (4) because of the simplifications of internal temperature gradients of spindle heat generating parts; On the other hand, $\frac{\mathrm{d}\Delta T_i}{\mathrm{d}\tau}\cong\Delta T_{i\_\tau+1}-\Delta T_{i\_\tau}\left(i=\mathrm{Fr},\mathrm{Mo},\mathrm{Ba}\right)$ can also be substituted into equation (4) to obtain its time discretization form. Consequently, equation (4) can be:

$$\frac{\Phi_{\mathrm{gen}\_i\_\tau+1}}{h_{\mathrm{coo}\_i}\Omega_i}+\Delta T_{\mathrm{coo}\_i\_\tau+1}=\frac{c_{\mathrm{T}\_i}}{h_{\mathrm{coo}\_i}\Omega_i}\bullet\left(\Delta T_{i\_\tau+1}-\Delta T_{i\_\tau}\right)+\Delta T_{i\_\tau}, i=\mathrm{Fr},\mathrm{Mo},\mathrm{Ba} \tag{5}$$

Then the time discretization model about spindle structural temperature can be:

$$\Delta T_{i\_\tau+1}=\frac{\Phi_{\mathrm{gen}\_i\_\tau+1}}{c_{\mathrm{T}\_i}+h_{\mathrm{coo}\_i}\Omega_i}+\frac{h_{\mathrm{coo}\_i}\Omega_i}{c_{\mathrm{T}\_i}+h_{\mathrm{coo}\_i}\Omega_i}\bullet\Delta T_{\mathrm{coo}\_i\_\tau+1}+\frac{c_{\mathrm{T}\_i}}{c_{\mathrm{T}\_i}+h_{\mathrm{coo}\_i}\Omega_i}\bullet\Delta T_{i\_\tau}, i=\mathrm{Fr},\mathrm{Mo},\mathrm{Ba} \tag{6}$$

2.1.2 Analytical modeling for spindle structural temperature – thermal deformation

Spindle thermal errors are generally attributed to thermal deformation of spindle structure. With the time discretization form, thermal deformation of spindle structure can be analyzed to be based on the thermal deformation ΔL of one dimensional rod with constraints [13]:

$$\begin{cases}\Delta L=\alpha L\left(\Delta T_{\tau+1}-\Delta T_{\tau}\right)+\dfrac{\sigma L}{E}\\ \Delta L=\dfrac{-P}{j}\\ P=A\sigma\end{cases} \tag{7}$$

In equation (7), L is original length (m); ΔT_{τ} and $\Delta T_{\tau+1}$ are rod temperatures at τ moment and τ+1 moment (℃); α is the thermal expansion coefficient (℃$^{-1}$); σ, P, E, j and A are the stress (MPa), the axial force (N), the modulus of elasticity (N/m^2), the axial stiffness (N/m) and the area of the cross section (m^2) respectively. Then the equation (7) can be simplified to be [13]:

$$\Delta L = \frac{\alpha L\left(\Delta T_{\tau+1} - \Delta T_{\tau}\right)}{1 + \frac{jL}{AE}} \tag{8}$$

Thus for the motorized spindle unit operating in the precision machining workshop, the thermal deformations of all spindle parts are caused by their time-varying temperatures. Then the fluctuation of spindle structural temperature can be attributed to the incomplete dissipations onto spindle heat generations. In other words, relative temperatures of spindle front bearings, motor and back bearing $\Delta T_{\mathrm{Fr/Mo/Ba}}\left(= T_{\mathrm{Fr/Mo/Ba}} - T_{\mathrm{am}}\right)$ are the dominant factors determining the spindle deformation errors, and should be perfectly regulated.

2.2 Analytical regulation measure onto coolant supply temperatures for constantly least spindle thermal errors

For the improvement of machining accuracy and accuracy stability, it is significant to reduce or eliminate spindle thermal errors by some effective ways. According to equation (8), thermal deformation errors of a motorized spindle unit in operation can be 0 theoretically only if spindle relative temperatures meet equation (9), with spindle initial temperatures being equal to 20℃ ambient temperature.

$$\Delta T_{i\_\tau+1} - \Delta T_{i\_\tau} = 0, i = \mathrm{Fr}, \mathrm{Mo}, \mathrm{Ba} \tag{9}$$

It can be concluded based on equation (6) that, there is a real time mapping relationship from $\Delta T_{i\_\tau} / \Phi_{\mathrm{gen}\_i\_\tau+1} / \Delta T_{\mathrm{coo}\_i\_\tau+1}$ to $\Delta T_{i\_\tau+1}$ $\left(i = \mathrm{Fr}, \mathrm{Mo}, \mathrm{Ba}\right)$ during the spindle operation. Because spindle heat generation powers are mainly affected by the spindle working rotation speed, the mapping relationship from $\Delta T_{i\_\tau} / n_{\tau+1} / \Delta T_{\mathrm{coo}\_i\_\tau+1}$ to $\Delta T_{i\_\tau+1}$ $\left(i = \mathrm{Fr}, \mathrm{Mo}, \mathrm{Ba}\right)$ can be trained by intelligent methods based on experimental data. Then the trained mapping model can be used as the active control algorithms onto thermal behaviors of motorized spindle unit. For a moment τ, spindle relative temperature $\Delta T_{\mathrm{Fr/Mo/Ba}\_\tau}$ and rotation speed $n_{\tau+1}$ can be detected based on RTD sensors and CNC communication technology respectively. Meanwhile, the relative coolant supply temperature $\Delta T_{\mathrm{coo\_Fr/Mo/Ba}\_\tau+1}$ must be determined based on an optimization method, whose objective is to minimize $\Delta T_{\mathrm{Fr/Mo/Ba}\_\tau+1}$. Then the further aim of this optimization is to realize equation (9), for the constant suppression onto spindle thermal errors. The construction of the active control algorithms above is described in Section 3.

3 Active and intelligent control algorithm onto spindle thermal behaviors

Based on theoretical analyses about the coolant supply temperature measure for constantly least spindle thermal errors above, this section introduces the construction of the active and intelligent control algorithm onto spindle thermal behaviors based on ELM and GA. This construction above includes the experimental model training of the active control algorithm and the optimization realization based on this pre-trained model.

3.1 OS-ELM based model training for active control algorithm onto spindle thermal behaviors

The experimental training of the active control algorithm is necessary for the realization of the active and intelligent control method onto spindle thermal behaviors. In this paper, online sequential extreme learning machine (OS-ELM) [23] is adopted for the model training of this active control algorithm. Firstly, being an advanced algorithm for training single-hidden layer feedforward neural networks (SLFN), the extreme learning machine (ELM) [23] determines randomly connection weights between input layer and hidden layer, and obtains connection weights between hidden layer and output layer by analytical method rather than iteratively tuning. Thus ELM can effectively avoid the slow training speed and local minimum problem suffered by the traditional neural network training algorithms. Secondly, being the vital ELM development, OS-ELM extends ELM for the online sequential training data. It even can learn the data one-by-one or chunk-by-chunk with fixed or varying chunk sizes.

For these advantages, OS-ELM is utilized to learn experimental online sequential mapping data, which reflect time-varying thermal behaviors of an operating motorized spindle unit. As reveled in Fig. 4, the applied SLFN has 3 input nodes, L hidden nodes and 1 output node. Then the output function of this SLFN can be:

$$f_L(\mathbf{x}) = \sum_{r=1}^{L} \beta_r G(\mathbf{a}_r, b_r, \mathbf{x}) \tag{10}$$

In equation (10):

$$\begin{cases} \mathbf{x}=\left[x_1,x_2,x_3\right]^{\mathrm{T}}=\left[\Delta T_{i\_\tau},n_{\tau+1},\Delta T_{\mathrm{coo}\_i\_\tau+1}\right]^{\mathrm{T}} \\ f_L\left(\mathbf{x}\right)=\Delta T_{i\_\tau+1} \end{cases},i=\mathrm{Fr},\mathrm{Mo},\mathrm{Ba} \tag{11}$$

Besides, $\mathbf{a}_r$ and b_r are learning parameters of hidden nodes, β_r is the output weight, and the activation function $G\left(\mathbf{a}_r,b_r,\mathbf{x}\right)$ denotes the output of r^{th} hidden node with respect to the input **x**. Based on this SLFN structure, OS-ELM training procedure is summarized as follows:

Step 1: Hidden parameters $\mathbf{a}_r$ and b_r $\left(r=1,2,...,L\right)$ of the applied SLFN are assigned randomly.

Step 2: For the model training of the active and intelligent control algorithm onto spindle thermal behaviors, the applied SLFN approximates a small chunk of detected training data $\aleph_0=\left\{\left(\mathbf{x}_\tau,t_\tau\right)\right\}_{\tau=1}^{N_0}$ with 0 error (N_0 is much larger than L.):

$$f_L\left(\mathbf{x}_\tau\right)=\sum_{r=1}^{L}\beta_r G\left(\mathbf{a}_r,b_r,\mathbf{x}_\tau\right)=\mathbf{t}_\tau,\tau=1,2,...,N_0 \tag{12}$$

Then equation (12) can be written compactly as:

$$\mathbf{H}_0\boldsymbol{\beta}_0=\mathbf{T}_0 \tag{13}$$

In equation (13):

$$\begin{cases} \mathbf{T}_0=\left[t_1,...,t_{N_0}\right]^{\mathrm{T}} \\ \mathbf{H}_0=\mathbf{H}\left(\mathbf{a}_1,...,\mathbf{a}_L,b_1,...,b_L,\mathbf{x}_1,...,\mathbf{x}_{N_0}\right)=\begin{bmatrix} G\left(\mathbf{a}_1,b_1,\mathbf{x}_1\right) & \cdots & G\left(\mathbf{a}_L,b_L,\mathbf{x}_1\right) \\ \vdots & \ddots & \vdots \\ G\left(\mathbf{a}_1,b_1,\mathbf{x}_{N_0}\right) & \cdots & G\left(\mathbf{a}_L,b_L,\mathbf{x}_{N_0}\right) \end{bmatrix}_{N_0\times L} \\ \boldsymbol{\beta}_0=\left[\beta_1^0,...,\beta_L^0\right]^{\mathrm{T}} \end{cases} \tag{14}$$

Step 3: The initial output weights can be calculated:

$$\boldsymbol{\beta}_0=\mathbf{P}_0\left(\mathbf{H}_0\right)^{\mathrm{T}}\mathbf{T}_0 \tag{15}$$

In equation (15):

$$\mathbf{P}_0 = \left(\left(\mathbf{H}_0 \right)^{\mathrm{T}} \mathbf{H}_0 \right)^{-1} \tag{16}$$

k=0.

Step 4: During the sequential model training stage of the active control algorithm onto spindle thermal behaviors, the applied SLFN approximates $(k+1)^{\text{th}}$ chunk of detected training data $\aleph_{k+1} = \left\{ \left(\mathbf{x}_\tau, \mathbf{t}_\tau \right) \right\}_{\tau=\left(\sum_{j=0}^{k} N_j\right)+1}^{\sum_{j=0}^{k+1} N_j}$ with 0 error (N_j is much larger than L.):

$$\sum_{r=1}^{L} \beta_r G\left(\mathbf{a}_r, b_r, \mathbf{x}_\tau \right) = \mathbf{t}_\tau, \tau = \left(\sum_{j=0}^{k} N_j \right) + 1, \left(\sum_{j=0}^{k} N_j \right) + 2, ..., \sum_{j=0}^{k+1} N_j \tag{17}$$

Then equation (17) can also be written compactly as:

$$\mathbf{H}_{k+1} \boldsymbol{\beta}_{k+1} = \mathbf{T}_{k+1} \tag{18}$$

In equation (18):

$$\begin{cases} \mathbf{T}_{k+1} = \left[t_{\left(\sum_{j=0}^{k} N_j\right)+1}, ..., t_{\sum_{j=0}^{k+1} N_j} \right]^{\mathrm{T}} \\ \mathbf{H}_{k+1} = \mathbf{H}\left(\mathbf{a}_1, ..., \mathbf{a}_L, b_1, ..., b_L, \mathbf{x}_{\left(\sum_{j=0}^{k} N_j\right)+1}, ..., \mathbf{x}_{\sum_{j=0}^{k+1} N_j} \right) = \begin{bmatrix} G\left(\mathbf{a}_1, b_1, \mathbf{x}_{\left(\sum_{j=0}^{k} N_j\right)+1} \right) & \cdots & G\left(\mathbf{a}_L, b_L, \mathbf{x}_{\left(\sum_{j=0}^{k} N_j\right)+1} \right) \\ \vdots & \ddots & \vdots \\ G\left(\mathbf{a}_1, b_1, \mathbf{x}_{\sum_{j=0}^{k+1} N_j} \right) & \cdots & G\left(\mathbf{a}_L, b_L, \mathbf{x}_{\sum_{j=0}^{k+1} N_j} \right) \end{bmatrix}_{\left(\sum_{j=0}^{k+1} N_j\right) \times L} \\ \boldsymbol{\beta}_{k+1} = \left[\beta_1^{k+1}, ..., \beta_L^{k+1} \right]^{\mathrm{T}} \end{cases} \tag{19}$$

Step 5: The sequential output weights can be calculated:

$$\boldsymbol{\beta}_{k+1} = \mathbf{P}_{k+1}\left(\mathbf{H}_{k+1}\right)^{\mathrm{T}}\mathbf{T}_{k+1} \tag{20}$$

In equation (20):

$$\mathbf{P}_{k+1} = \left(\left(\mathbf{H}_{k+1}\right)^{\mathrm{T}}\mathbf{H}_{k+1}\right)^{-1} = \mathbf{P}_k - \mathbf{P}_k\left(\mathbf{H}_{k+1}\right)^{\mathrm{T}}\left(I + \mathbf{H}_{k+1}\mathbf{P}_k\left(\mathbf{H}_{k+1}\right)^{\mathrm{T}}\right)^{-1}\mathbf{H}_{k+1}\mathbf{P}_k \tag{21}$$

$\boldsymbol{\beta}_k = \mathbf{P}_k\left(\mathbf{H}_k\right)^{\mathrm{T}}\mathbf{T}_k$ is considered into equation (21) to obtain:

$$\boldsymbol{\beta}_{k+1} = \boldsymbol{\beta}_k + \mathbf{P}_{k+1}\left(\mathbf{H}_{k+1}\right)^{\mathrm{T}}\left(\mathbf{T}_{k+1} - \mathbf{H}_{k+1}\boldsymbol{\beta}_k\right) \tag{22}$$

If another chunk of new training data is presented, then k=k+1 and return to Step 4; If no training data comes, then denote the last iteration output weights as $\boldsymbol{\beta}$:

$$\boldsymbol{\beta} = \left[\beta_1, ..., \beta_L\right]^{\mathrm{T}} \tag{23}$$

With the obtained $\boldsymbol{\beta}$ above, the SLFN output function represented in equation (10) can be applied as the pre-trained predictive model for the active control algorithm onto spindle thermal behaviors.

3.2 ELM-GA based active control algorithm for spindle thermal behaviors

3.2.1 Optimization method of active control algorithm for spindle thermal behaviors

Based on the pre-trained ELM predictive model for the active control algorithm onto spindle thermal behaviors, the optimization regulation of this algorithm can be realized based on the principle illustrated in Fig. 5: During the spindle operation, the detected spindle structural temperatures, rotation speed and coolant supply temperatures are dynamically used to predict spindle structural temperatures. For these 3 necessary input variables for the active control algorithm onto spindle thermal behaviors, the former 2 variables are obtained based on real-time detections during the spindle operation, and the latter one must be dynamically regulated by an optimization method, to minimize the predicted relative spindle structural temperature to ambient temperature (20℃), thus to cut down spindle thermal errors. In this paper, the genetic algorithm (GA) method is adopted to construct this active control algorithm.

3.2.2 ELM predictive model based GA active control algorithm for spindle thermal behaviors

Being an effective random search method for global optimum, genetic algorithm (GA) uses a population of strings to encode the initial candidate solutions. And then it employs genetic operators, including selection, mutation and crossover, to generate new populations based on the initial population, and gradually evolves towards the best solution [24]. The main advantages of GA include its strong robustness, convergence to global optimum and parallel search capability. Owing to these advantages, GA can be appropriately adopted for the dynamic optimization regulation onto relative supply temperatures $\Delta T_{\mathrm{coo\_Fr/Mo/Ba}\_\tau+1}$ of spindle coolants, based on the pre-trained ELM predictive model obtained in Section 3.1. The optimization objective of GA active control algorithm is as follows:

$$J = \min\left(\left|\Delta T_{i\_\tau+1}\right|\right), i = \mathrm{Fr}, \mathrm{Mo}, \mathrm{Ba} \tag{24}$$

As depicted in Fig. 6, the dynamic optimization and updating of $\Delta T_{\mathrm{coo\_Fr/Mo/Ba}\_\tau+1}$ at any moment τ can be realized based on GA method by following steps:

Step 1: For any moment τ of the spindle operation, the prerequisite to launch the dynamic optimization about parameters $\Delta T_{\mathrm{coo\_Fr/Mo/Ba}\_\tau+1}$ of the ELM-GA based active control algorithm is constructed based on any continuous M observations onto $\Delta T_{\mathrm{Fr/Mo/Ba}}$ ($\boldsymbol{A}$) from moment τ-(M-1) to τ:

$$\boldsymbol{A} = \left[\Delta T_{i\_\tau-(M-1)}, \ldots, \Delta T_{i\_\tau-1}, \Delta T_{i\_\tau}\right], i = \mathrm{Fr}, \mathrm{Mo}, \mathrm{Ba} \tag{25}$$

Coolant relative supply temperatures $\Delta T_{\mathrm{coo\_Fr/Mo/Ba}\_\tau+1}$ should not be optimized and updated at moment τ+1, only if the continuous M observations above meet the prerequisite at moment τ:

$$\frac{1}{M}\sum_{k=1}^{M}\left|\Delta T_{i\_k}\right| \le A^{\mathrm{sta}}, i = \mathrm{Fr}, \mathrm{Mo}, \mathrm{Ba}; k = \tau-(M-1), \ldots, \tau-1, \tau \tag{26}$$

In equation (26), A^{sta} is the given tolerance for the average values of continuous *M* absolute values of observed $\Delta T_{\text{Fr/Mo/Ba}}$. If these average values cannot meet the prerequisite of equation (26) at moment τ, coolant relative supply temperatures $\Delta T_{\text{coo\_Fr/Mo/Ba\_}\tau+1}$ should be updated by GA optimization method at moment τ+1 (turn to Step 2).

Step 2: Coolant relative supply temperatures $\Delta T_{\text{coo\_Fr/Mo/Ba\_}\tau}$ are used to construct their generation ranges for GA optimization method:

$$D_{\text{coo\_}i} = \left[\Delta T_{\text{coo\_}i\text{\_}\tau} - \delta_{\text{coo\_}i}^{\text{low}}, \Delta T_{\text{coo\_}i\text{\_}\tau} + \delta_{\text{coo\_}i}^{\text{up}}\right], i = \text{Fr}, \text{Mo}, \text{Ba} \tag{27}$$

In equation (27), $\delta_{\text{coo\_Fr/Mo/Ba}}^{\text{up}}$ and $\delta_{\text{coo\_Fr/Mo/Ba}}^{\text{low}}$ are upper and lower deviations for the random generation of coolant relative supply temperatures $\Delta T_{\text{coo\_Fr/Mo/Ba}}$. According to these ranges, 1st *N* solutions of $\Delta T_{\text{coo\_Fr/Mo/Ba\_}\tau+1}$ are generated randomly; *Gen*=1.

Step 3: *Gen*th solutions $\Delta T_{\text{coo\_Fr/Mo/Ba\_}\tau+1}^{(Gen\text{-}1)\bullet N+\theta}, \theta = 1, 2, ..., N$ are used respectively to be together with the currently detected spindle structural temperature $\Delta T_{\text{Fr/Mo/Ba\_}\tau}$ and rotation speed $n_{\tau+1}$, to predict spindle structural temperature $\Delta T_{\text{Fr/Mo/Ba\_}\tau+1}$ by the pre-trained ELM model.

Step 4: The obtained $\Delta T_{\text{Fr/Mo/Ba\_}\tau+1}^{(Gen\text{-}1)\bullet N+\theta}, \theta = 1, 2, ..., N$ are substituted into equation (24) for GA fitness evaluations of $\Delta T_{\text{coo\_Fr/Mo/Ba\_}\tau+1}^{(Gen\text{-}1)\bullet N+\theta}, \theta = 1, 2, ..., N$.

Step 5: The dynamic GA optimization is terminated only if $\Delta T_{\text{Fr/Mo/Ba\_}\tau+1}^{(Gen\text{-}1)\bullet N+\theta'}$ meet the following prerequisite:

$$\left|\Delta T_{i\_\tau+1}^{(Gen\text{-}1)\bullet N+\theta'}\right| \le A^{\text{sta}}, i = \text{Fr}, \text{Mo}, \text{Ba} \tag{28}$$

In equation (28), θ' is the sequence number of the solution with the highest fitness value from *Gen*th solutions. If the dynamic GA optimization is terminated, to perform Step 6; if not, to evaluate whether the following prerequisite is met:

$$Gen \ge MaxGen \tag{29}$$

In equation (29), $MaxGen$ is the upper limit for GA generation number. If the prerequisite of equation (29) is met, to terminate dynamic GA optimization and to perform Step 6; if not, to perform Step 7.

Step 6: The solution with the highest fitness value $\Delta T_{\text{coo\_Fr/Mo/Ba\_}\tau+1}^{(Gen\text{-}1)\bullet N+\theta'}$ from Gen^{th} solutions is used as the updated coolant relative supply temperature. The aim is for ongoing active and differentiated control onto spindle thermal behaviors:

$$\Delta T_{\text{coo\_Fr/Mo/Ba\_}\tau+1} = \Delta T_{\text{coo\_Fr/Mo/Ba\_}\tau+1}^{(Gen\text{-}1)\bullet N+\theta'} \tag{30}$$

Step 7: Gen^{th} solutions are encoded to generate Gen^{th} population. According to equation (27) and the evolution direction provided by the evaluated fitness values of Gen^{th} solutions, GA employs genetic operators (selection, mutation and crossover) to generate $(Gen+1)^{\text{th}}$ population based on Gen^{th} one. Then $(Gen+1)^{\text{th}}$ population is decoded to construct $(Gen+1)^{\text{th}}$ solutions.

Step 8: $Gen=Gen+1$, and turn to Step 3.

4 Experiments

The advantages of the proposed active and intelligent control method onto thermal behaviors of motorized spindle unit are investigated experimentally in this section. Based on the constructed monitor-active control platform for spindle thermal behaviors, the advantages of this proposed method in spindle thermal error suppression can be verified by the method of contrasting experiments.

4.1 Monitor – active control platform for spindle thermal behaviors

4.1.1 Construction of monitor – active control platform for spindle thermal behaviors

As illustrated in Fig. 7, the monitor – active control platform for thermal behaviors of motorized spindle unit is established based on the differentiated multi-loops bath recirculation system [25] and necessary thermal sensors for motorized spindle unit. Firstly, internal coolant channels of motorized spindle unit are equipped with the differentiated multi-loops bath recirculation system, which is the preparation for the differentiated and dynamic cooling method onto spindle heat generating parts. Besides, temperature signals (from the located RTD sensors) and thermal error signals (from eddy current displacement sensors) are collected by signal acquisition system, and conveyed to the host computer software. In this software, the real-time temperature and thermal error signals are displayed in the monitoring module during the spindle operation. Meanwhile, the spindle rotation speed can be detected by CNC communication method, and conveyed to the host computer software as well. The spindle structural temperature and rotation speed detections are used to trigger ELM-GA based active control algorithms, which are introduced in Section 3, in the controlling module of the software to generate coolant supply temperature instructions. And these instructions are conveyed to the differentiated multi-loops bath recirculation system by communication unit (USB converted to RS485) for real-time regulations onto coolant supply temperatures.

In the monitor - active control platform for spindle thermal behaviors, the structural temperatures and thermal errors of motorized spindle unit are designed to be measured by RTD sensors and eddy current displacement sensors respectively. As revealed in Fig. 7, the layouts of these 2 kinds of thermal sensors can be described as follows: On one hand, RTD sensors are located nearby spindle heat generating parts: T_A and T_B are measured to be the temperature of front bearings; T_C-T_F stand for the motor temperature; T_G and T_H are used for detecting the back bearing temperature. Then the final experimental values of spindle front bearings temperature T_{Fr}, motor temperature T_{Mo} and back bearing temperature T_{Ba} can be obtained based on the average values of the detections from RTD sensors T_A / T_B, T_C-T_F and T_G / T_H respectively:

$$\begin{cases} T_{\mathrm{Fr}} = \dfrac{1}{2}\left(T_{\mathrm{A}} + T_{\mathrm{B}}\right) \\ T_{\mathrm{Mo}} = \dfrac{1}{4}\left(T_{\mathrm{C}} + T_{\mathrm{D}} + T_{\mathrm{E}} + T_{\mathrm{F}}\right) \\ T_{\mathrm{Ba}} = \dfrac{1}{2}\left(T_{\mathrm{G}} + T_{\mathrm{H}}\right) \end{cases} \tag{31}$$

On the other hand, spindle thermal errors are detected by eddy current displacement sensors based on inspection bar, the location of eddy current displacement sensors must be according to the standard method of spindle thermal errors [26]. Based on the geometry relationship revealed in Fig. 7, spindle linear thermal error $\overline{\delta_Z}$ can be obtained directly from axial eddy current displacement sensor, and angular thermal errors $\overline{\varepsilon_X} / \overline{\varepsilon_Y}$ and linear thermal errors $\overline{\delta_X} / \overline{\delta_Y}$

must be calculated based on detected values from eddy current displacement sensors X(A)/ Y(A)/ X(B)/ Y(B) by following methods respectively:

$$\begin{cases} \overline{\varepsilon_{\mathrm{X}}} = \tan^{-1}\left(\dfrac{\overline{\delta_{\mathrm{X(A)}}} - \overline{\delta_{\mathrm{X(B)}}}}{L_{\mathrm{BA}}}\right) \\ \overline{\varepsilon_{\mathrm{Y}}} = \tan^{-1}\left(\dfrac{\overline{\delta_{\mathrm{Y(A)}}} - \overline{\delta_{\mathrm{Y(B)}}}}{L_{\mathrm{BA}}}\right) \end{cases} \tag{32}$$

$$\begin{cases} \overline{\delta_{\mathrm{X}}} = \dfrac{\overline{\delta_{\mathrm{X(A)}}} - \dfrac{L_{\mathrm{OA}}}{L_{\mathrm{OB}}}\overline{\delta_{\mathrm{X(B)}}}}{(1-\dfrac{L_{\mathrm{OA}}}{L_{\mathrm{OB}}})} \\ \overline{\delta_{\mathrm{Y}}} = \dfrac{\overline{\delta_{\mathrm{Y(A)}}} - \dfrac{L_{\mathrm{OA}}}{L_{\mathrm{OB}}}\overline{\delta_{\mathrm{Y(B)}}}}{(1-\dfrac{L_{\mathrm{OA}}}{L_{\mathrm{OB}}})} \end{cases} \tag{33}$$

4.1.2 Spindle coolant channels equipped with differentiated multi-loops bath recirculation system

In order to verify advantages of the proposed active, differentiated and intelligent control method onto spindle thermal behaviors, the motorized spindle unit is required to be equipped with the differentiated multi-loops bath recirculation system, which is developed in our previous study [25]. Because there are 3 helical coolant channels (for front bearings, motor and back bearing) inside motorized spindle unit, 3 recirculation branches of this system are adopted in this study. As illustrated in Fig. 8, 2 recirculation coolers are in 2 recirculation trunks respectively to supply recirculation coolants of high and low temperatures respectively; recirculation branches are equipped with independent coolant blenders to supply recirculation coolants of differentiated and dynamic supply temperatures onto coolant channels via spindle front bearings, motor and back bearing respectively. The differentiated coolant supply temperatures are realized by real-time blending ratio regulations of recirculation coolants from 2 recirculation coolers, and this ratio is controlled by the open ranges of input and output electric valve groups.

4.2 Method of experimental verifications

Based on the monitor - active control platform above, spindle thermal behaviors can be monitored during spindle operations under 2 distinct spindle cooling strategies respectively: active and intelligent control method and traditional cooling method (The coolant supply temperature is always equivalent to ambient temperature 20℃). For both the different cooling methods above, the supply volume flow rate of every recirculation coolant is 5L/min. In precision machining environment (with a consistent room temperature T_{am}=20±0.3℃), all the experimental operations of motorized spindle unit last for 5 hours. Based on the contrasting experiments above, the experimental thermal behaviors (temperature and thermal errors) of motorized spindle unit caused by the active and intelligent control method will be contrasted with the ones caused by traditional cooling method.

Specially, the contrasting experiments are done in 2 spindle operating conditions respectively: constant and progressive rotation speed cases. In the constant rotation speed case, the motorized spindle unit is in 3000RPM operation for 5 hours; but in the progressive rotation speed case, the spindle is operating from 2000RPM to 4000RPM (the increasing step length of spindle rotation speed is 500RPM, and every rotation speed lasts for 1 hour).

4.3 Experimental Results and Discussions

4.3.1 Spindle structural temperatures

It can be seen from Fig. 9 (a) that, in spindle progressive rotation speed case, the coolant supply temperatures caused by the traditional cooling method are constantly equal to ambient temperature (20±0.3℃), and the caused structural temperatures of motorized spindle unit are different and obviously increasing with time. Oppositely, in Fig. 9 (b), the presented active and intelligent control method makes various and time-varying coolant supply temperatures onto different spindle heat generating parts, but spindle structural temperatures are more consistent and close to room temperature. That shows: the active and intelligent control method is more effective than traditional cooling method in spindle structural temperature stabilization. This can be concluded from constant rotation speed case of motorized spindle unit as well.

4.3.2 Spindle Thermal Errors

Fig. 10 shows experimental contrasting results of spindle thermal errors caused by the active and intelligent control method and the traditional cooling method (in progressive rotation speed cases). It can be seen from the figures that, 5 kinds of spindle thermal errors are increasing with time. Meanwhile, the maximum values of 5 thermal errors caused by the active and intelligent control method are lower than the ones caused by the traditional cooling method in different degrees. This condition can also be concluded in both the constant and progressive rotation speed cases, and the reducing percentages of spindle thermal errors are listed in Table. 1. Consequently, compared with the traditional cooling method, the active and intelligent control method can obviously reduce spindle thermal errors, and contribute to the comprehensive accuracy improvement of precision machining activities.

Furthermore, compared with thermal error compensation method, the active and intelligent control method is more beneficial for improvements of spindle accuracy and accuracy stability as well. That is because the active and intelligent control method can experimentally realize the comprehensive suppression onto 5 kinds of spindle thermal errors, but the inherent shortage of the compensation method is its inability to compensate for spindle thermal errors in the freedom degrees excluded by machine drive system.

5 Conclusions

For promoting the accuracy and accuracy stability of motorized spindle unit, this paper introduces an active, differentiated and intelligent control method onto spindle thermal behaviors. This method is proposed based on the mechanism of spindle heat generation/ dissipation - structural temperature - thermal deformation errors, and realized by GA dynamic optimization method with a pre-trained ELM predictive model. In summary, conclusions of this paper are as follows:

1) The presented active and intelligent control method onto spindle thermal behaviors can effectively realize accurate suppressions onto 5 kinds of spindle thermal errors, which is verified by experiments. Compared with thermal error compensation method, this method is more advantageous in the improvements of accuracy and accuracy stability of motorized spindle unit.

2) The ELM-GA based active control algorithm can effectively realize the stabilization regulation onto spindle structural temperature, despite differentiated and time-varying heat generations to disturb spindle temperature. It can be experimentally verified that, ELM-GA based active control algorithm is more advantageous than traditional cooling strategy in spindle temperature stabilization.

Acknowledgment

The authors acknowledge the National Science and Technology Major Project of China (No. 2018ZX04031002), the Fund of Nature Science Foundation in Tianjin of China (No. 17JCZDJC40300), the Youth Talent Program of Higher Education Institutions in Hebei Province of China (No. BJ2017039), the Youth Fund of Natural Science Foundation in Hebei Province of China (No. E2017202194), and the "Chunhui Plan" Cooperative Project of Education Ministry of China (No. Z2017011).

References

[1] Li Y, Zhao WH, Lan SH, Ni J, Wu WW, Lu BH (2015) A review on spindle thermal error compensation in machine tools. Int J Mach Tools Manuf 95: 20-38

[2] Holkup T, Cao H, Kolar P, Altintas Y, Zeleny J (2010) Thermo-mechanical model of spindles. CIRP Ann - Manuf Technol 59 (1): 365-368

[3] Jiang SY, Mao HB (2010) Investigation of variable optimum preload for a machine tool spindle. Int J Mach Tools Manuf 50 (1): 19-28

[4] Creighton E, Honegger A, Tulsian A, Mukhopadhyay D (2010) Analysis of thermal errors in a high-speed micro-milling spindle. Int J Mach Tools Manuf 50 (4): 386-393

[5] Zheng EL, Jia F, Zhu SH (2014) Thermal modeling and characteristics analysis of high speed press system. Int J Mach Tools Manuf 85 (7): 87-99

[6] Ma C, Yang J, Zhao L, Mei XS, Shi H (2015) Simulation and experimental study on the thermally induced deformations of high-speed spindle system. Appl Therm Eng 86: 251-268

[7] Liu ZF, Pan MH, Zhang AP, Zhao YS, Yang Y, Ma CY (2015) Thermal characteristic analysis of high-speed motorized spindle system based on thermal contact resistance and thermal-conduction resistance. Int J Adv Manuf Tech 76 (9): 1913-1926

[8] Denis Ashok S, Samuel GL (2012) Modeling, measurement, and evaluation of spindle radial errors in a miniaturized machine tool. Int J Adv Manuf Tech 59 (5): 445-462

[9] Prashanth Anandan K, Burak Ozdoganlar O (2013) Analysis of error motions of ultra-high-speed (UHS) micromachining spindles. Int J Mach Tools Manuf 70: 1-14

[10] Ibaraki S, Ota Y (2014) A machining test to calibrate rotary axis error motions of five-axis machine tools and its application to thermal deformation test. Int J Mach Tools Manuf 86: 81-88

[11] Huang YQ, Zhang J, Li X, Tian LJ (2014) Thermal error modeling by integrating GA and BP algorithms for the high-speed spindle. Int J Adv Manuf Tech 71 (9): 1669-1675

[12] Wang BM, Mei XS, Wu ZX, Zhu F (2015) Dynamic modeling for thermal error in motorized spindles. Int J Adv Manuf Tech 78 (5): 1141-1146

[13] Li Y, Zhao WH, Wu WW, Lu BH, Chen YB (2014) Thermal error modeling of the spindle based on multiple variables for the precision machine tool. Int J Adv Manuf Tech 72 (9): 1415-1427

[14] Ni J (1997) CNC machine accuracy enhancement through real-time error compensation. J Manuf Sci Eng-Trans ASME 119: 717–725

[15] Mayr J, Jedrzejewski J, Uhlmann E, Alkan Donmez M, Knapp W, Hartig F, Wendt K, Moriwaki T, Shore P, Schmitt R, Brecher C, Wurz T, Wegener K (2012) Thermal issues in machine tools. CIRP Ann - Manuf Technol 61 (2): 771-791

[16] Jedrzejewski J (1988) Effect of the thermal contact resistance on thermal behavior of the spindle radial bearings. Int J Mach Tools Manuf 28 (4): 409-416

[17] Chang CF, Chen JJ (2009) Thermal growth control techniques for motorized spindles.

Mechatronics 19: 1313–1320

[18] Shen HY, Fu JZ, He Y, Yao XH (2012) On-line asynchronous compensation methods for static/quasi-static error implemented on CNC machine tools. Int J Mach Tools Manuf 60: 14-26

[19] Gomez-Acedo E, Olarra A, Orive J, de Lacalle LNL (2013) Methodology for the design of a thermal distortion compensation for large machine tools based in state-space representation with Kalman filter. Int J Mach Tools Manuf 75 (12): 100-108

[20] Yang J, Shi H, Feng B, Zhao L, Ma C, Mei XS (2015) Thermal error modeling and compensation for a high-speed motorized spindle. Int J Adv Manuf Tech 77: 1005–1017

[21] Mayr J, Egeter M, Weikert S, Wegener K (2015) Thermal error compensation of rotary axes and main spindles using cooling power as input parameter. J Manuf Syst 37: 542–549

[22] Liu K, Sun MJ, Zhu TJ, Wu YL, Liu Y (2016) Modeling and compensation for spindle's radial thermal drift error on a vertical machining center. Int J Mach Tools Manuf 105: 58-67

[23] Huang GB, Zhu QY, Siew CK (2006) Extreme learning machine: theory and applications, Neurocomputing 70 (1-3): 489–501

[24] Goldberg D E (1989) Genetic algorithm in search, optimization and machine learning, Addison-Wesley. Massachusetts

[25] Liu T, Gao WG, Tian YL, Zhang HJ, Chang WF, Mao K, Zhang DW (2015) A differentiated multi-loops bath recirculation system for precision machine tools. Appl Therm Eng 76c: 54-63

[26] ISO 230-3-2007. Test code for machine tools - Part 3: Determination of thermal effects (Second Edition)

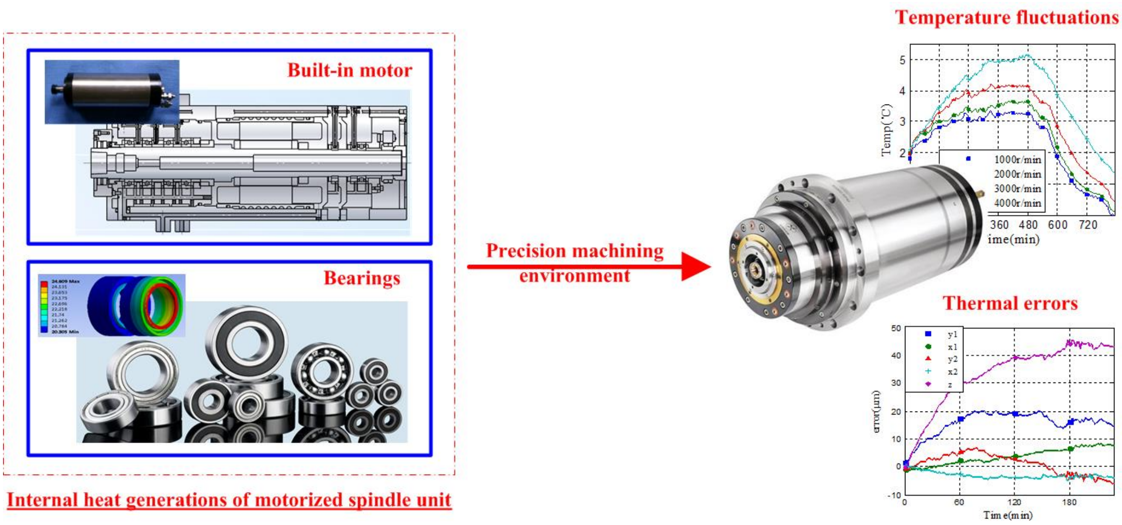

Fig. 1 Thermal analysis of a motorized spindle unit in operation

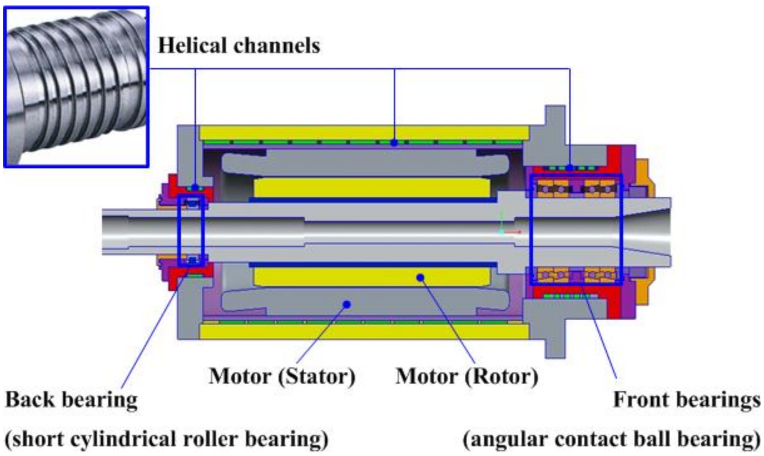

Fig. 2 Heat generating parts and helical channels of motorized spindle unit

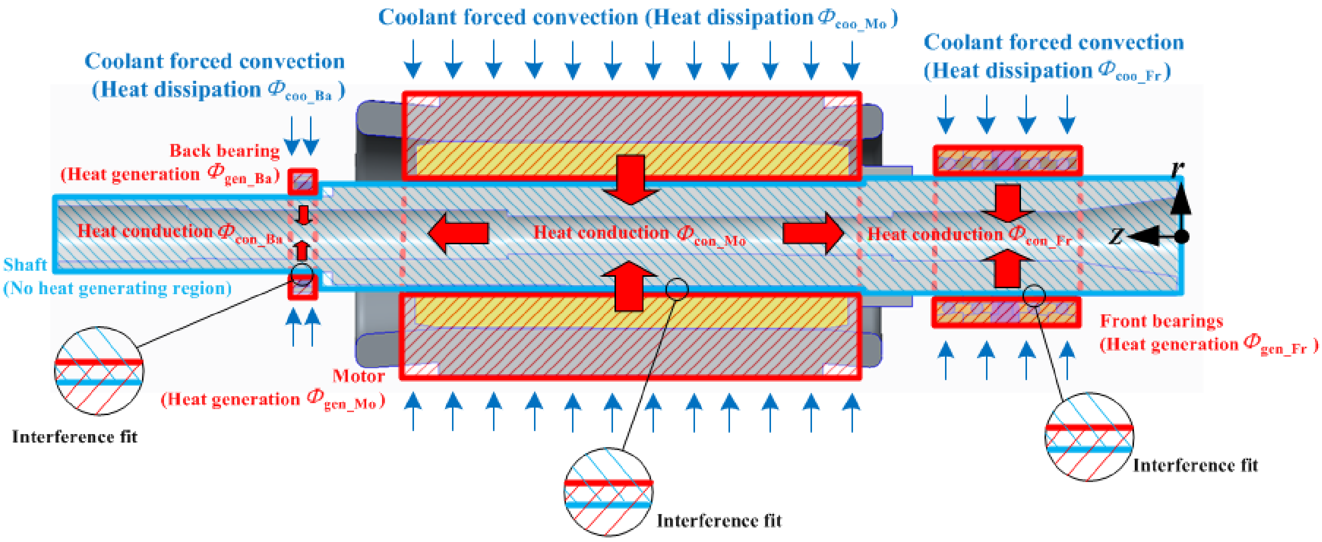

Fig. 3 Spindle heat exchange analyses based on a simplified spindle structure

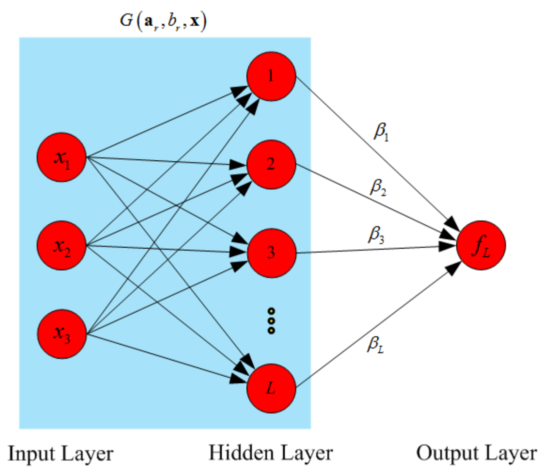

Fig. 4 Structure of the applied SLFN with 3 input nodes, L hidden nodes and 1 output node

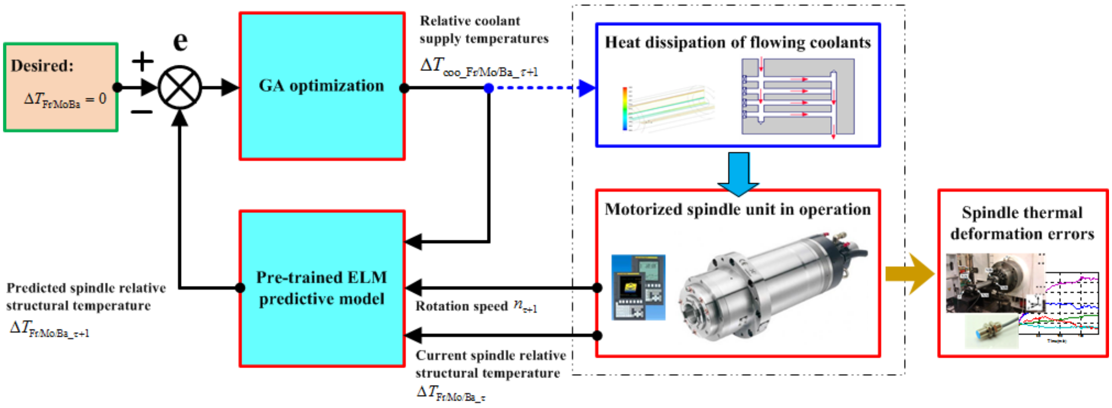

Fig. 5 Principle of the active and intelligent control method onto spindle thermal behaviors

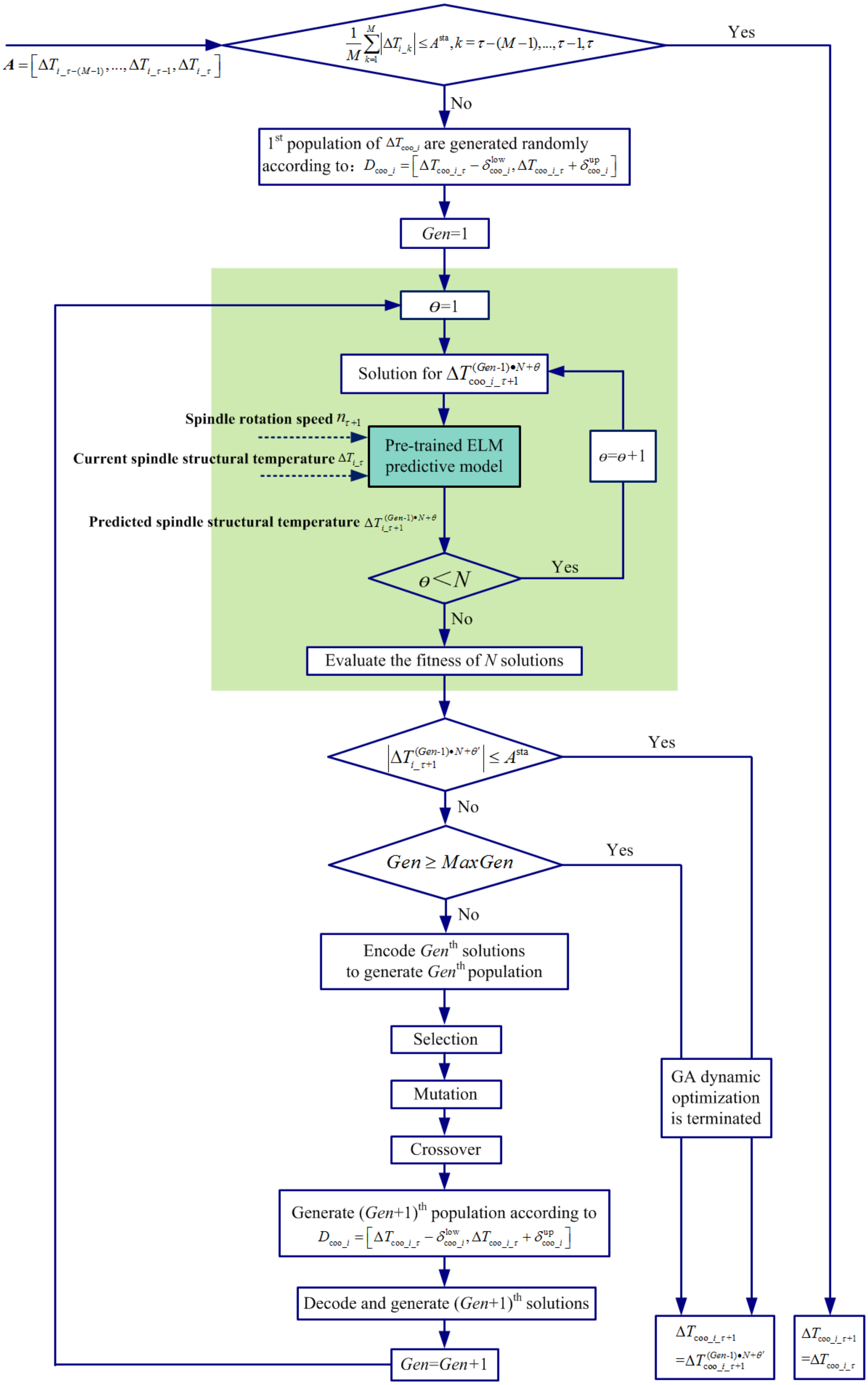

Fig. 6 Procedure of GA dynamic optimization about $\Delta T_{\mathrm{coo}\_i}$ (i=Fr, Mo, Ba)

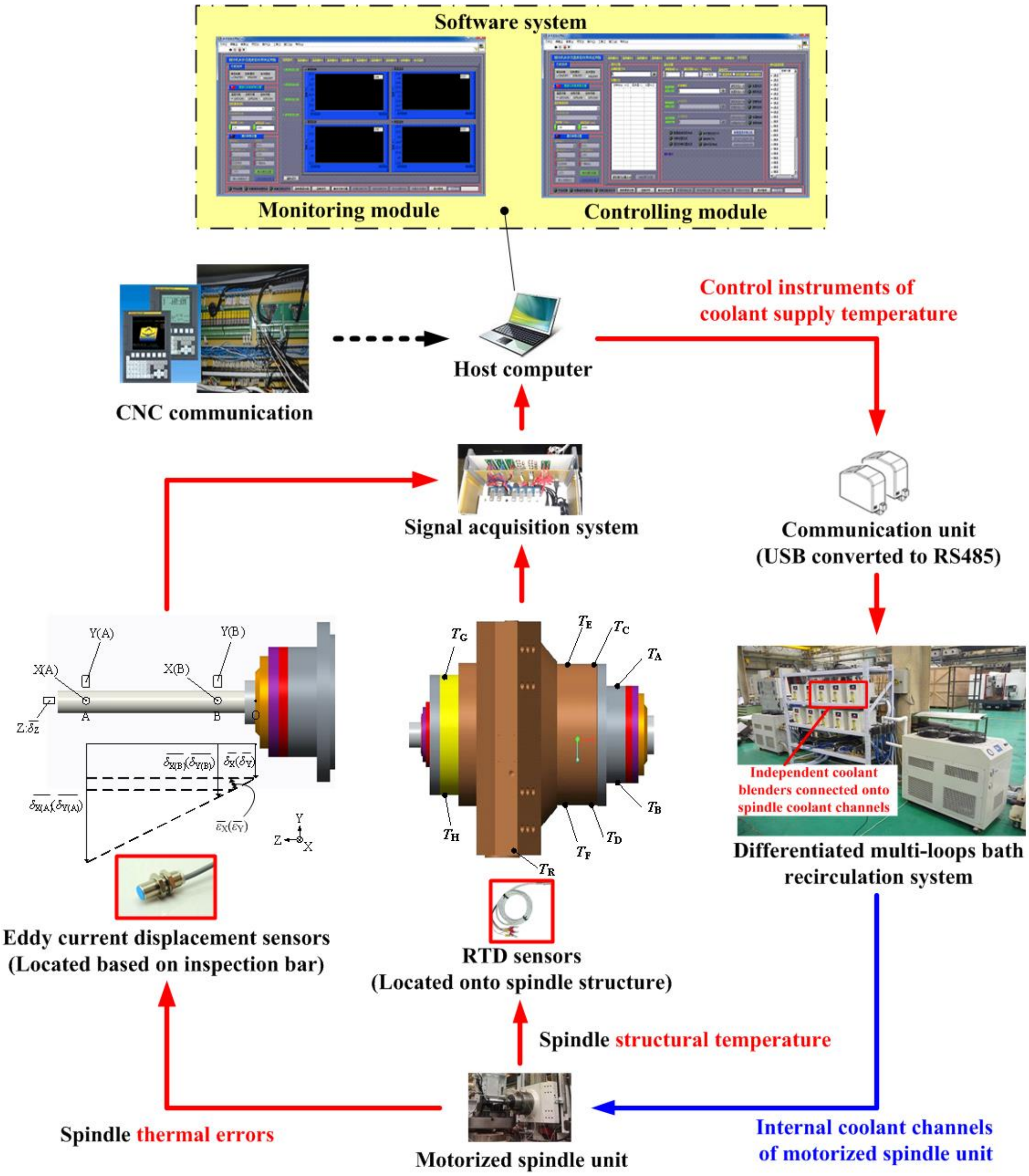

Fig. 7 Structure of monitor – active control platform for thermal behaviors of motorized spindle unit

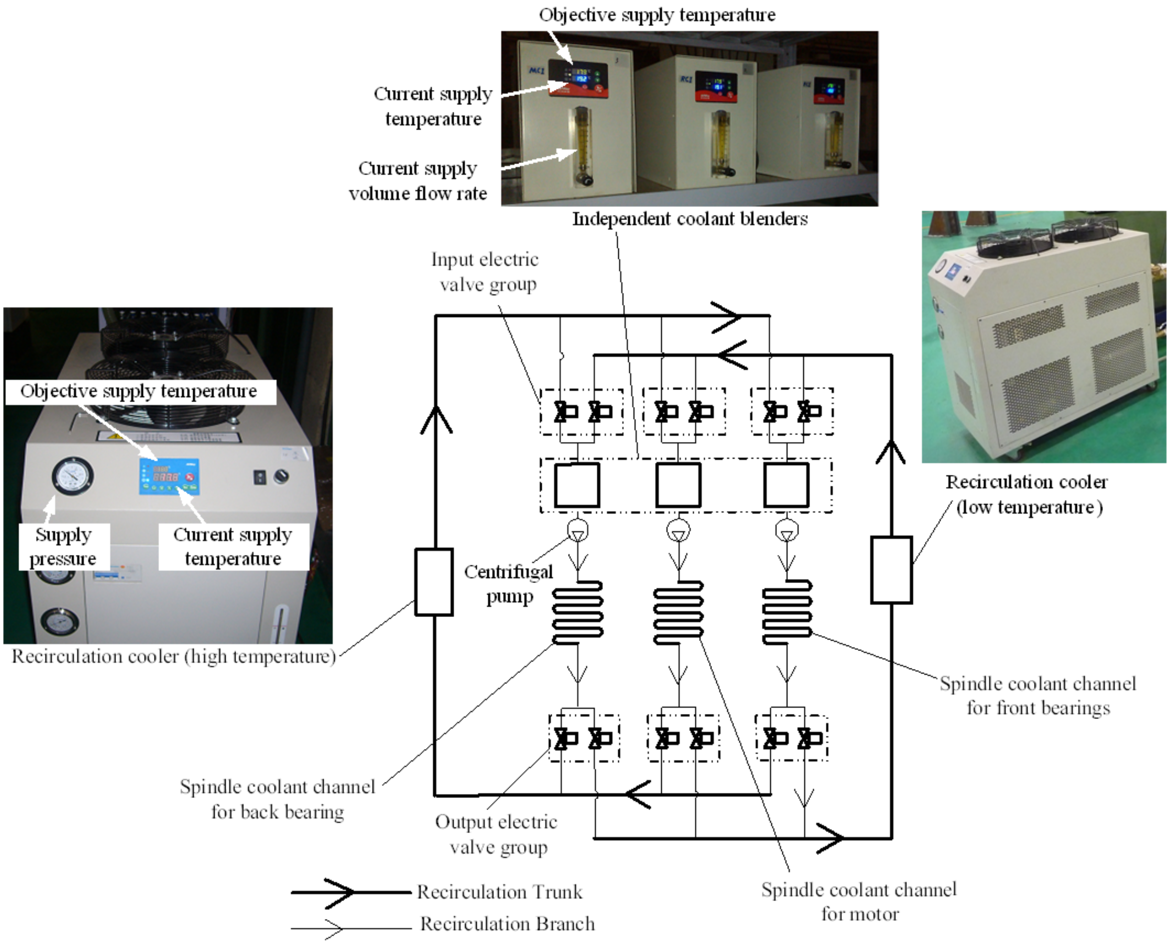

Fig.8 Spindle coolant channels equipped with the differentiated multi-loops bath recirculation system

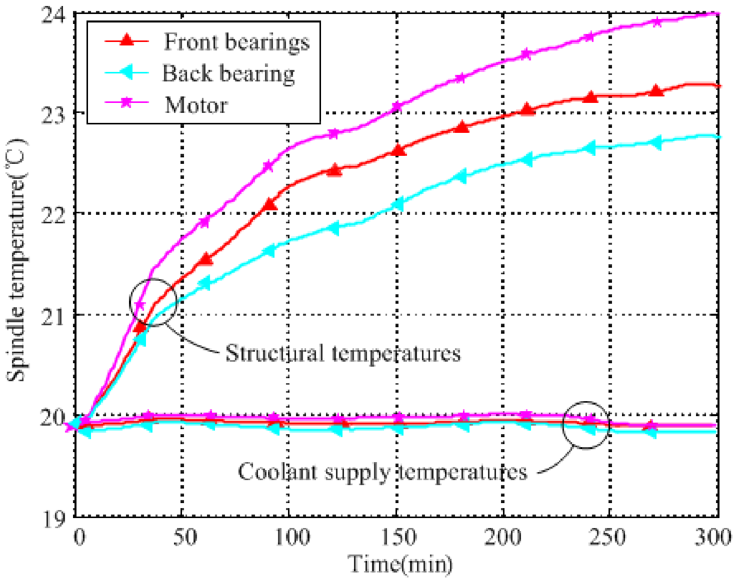

(a) Traditional cooling method

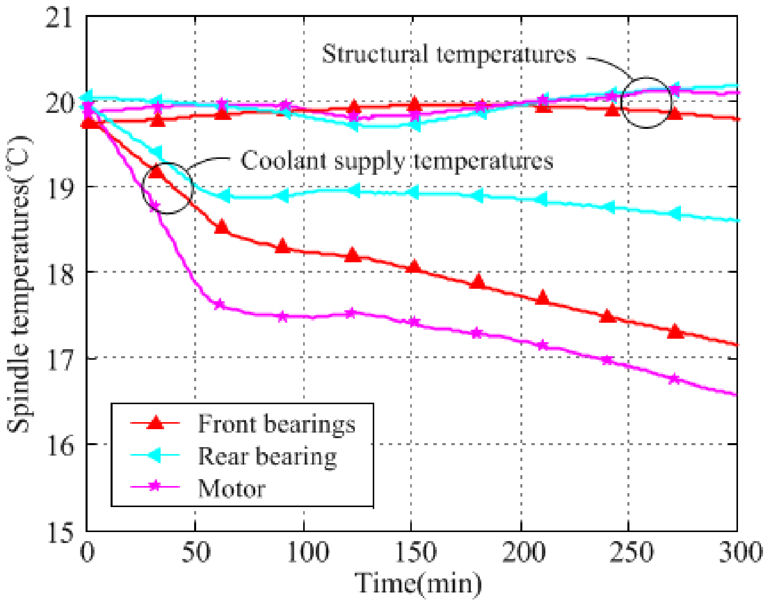

(b) Active and intelligent control method

Fig. 9 Coolant supply temperatures and spindle structural temperatures detected in contrasting experiments (Progressive rotation speed case)

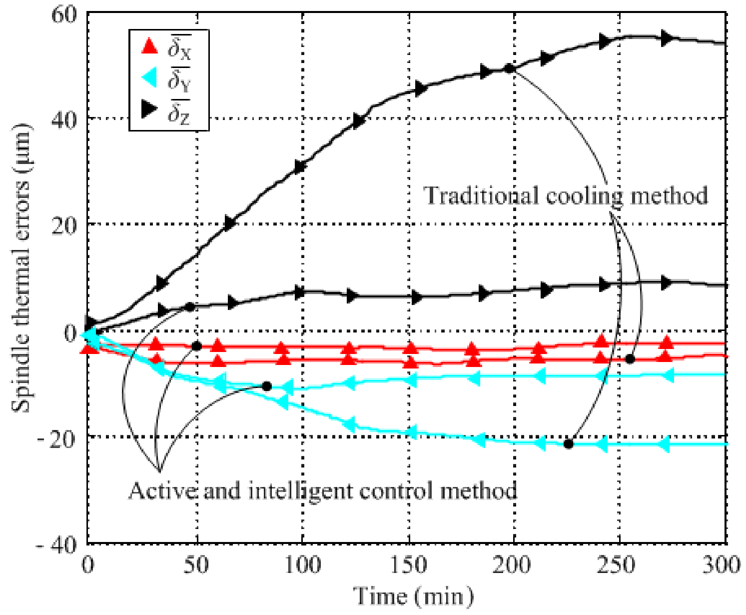

(a) Linear thermal errors

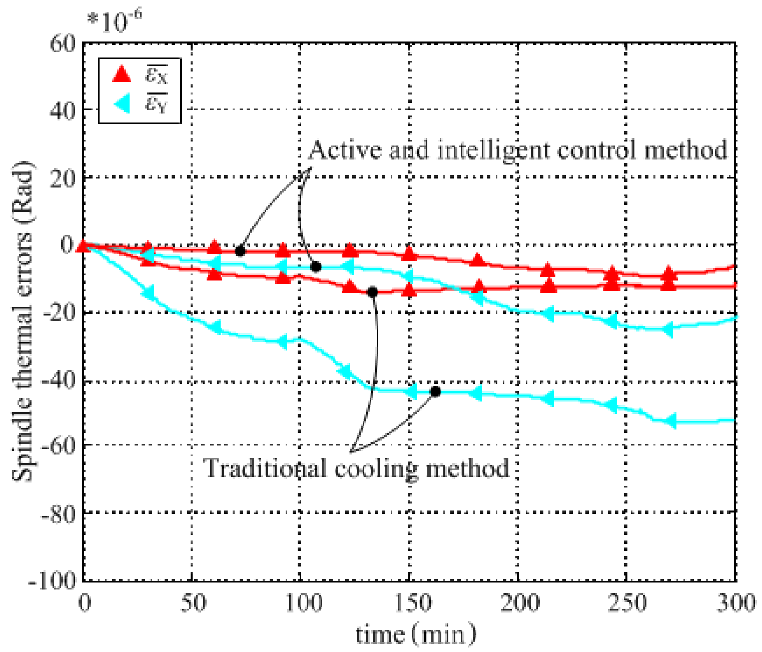

(b) Angular thermal errors

Fig. 10 Thermal errors of motorized spindle unit detected in contrasting experiments (Progressive rotation speed case)

Table 1. Reducing percentages of spindle thermal errors caused by the active and intelligent control method (contrasted with traditional cooling method)

	$\overline{\delta_X}$	$\overline{\delta_Y}$	$\overline{\delta_Z}$	$\overline{\varepsilon_X}$	$\overline{\varepsilon_Y}$
Constant rotation speed case	41.3%	54.3%	88.4%	30.1%	58.2%
Progressive rotation speed case	36.9%	46.7%	81.9%	27.6%	54.5%